Journal of Photonics for Energy

PhotonicsforEnergy.SPIEDigitalLibrary.org

Funneling and guiding effects in ultrathin aSi-H solar cells using one-dimensional dielectric subwavelength gratings

Mahmoud H. Elshorbagy
Javier Alda

SPIE.

Mahmoud H. Elshorbagy, Javier Alda, "Funneling and guiding effects in ultrathin aSi-H solar cells using one-dimensional dielectric subwavelength gratings," *J. Photon. Energy* **7**(1), 017002 (2017), doi: 10.1117/1.JPE.7.017002.

Funneling and guiding effects in ultrathin aSi-H solar cells using one-dimensional dielectric subwavelength gratings

Mahmoud H. Elshorbagy[a,b] and Javier Alda[a,*]
[a]University Complutense of Madrid, Applied Optics Complutense Group, Faculty of Optics and Optometry, Madrid, Spain
[b]Minia University, Physics Department, Faculty of Science, El-Minya, Egypt

Abstract. Ultrathin amorphous silicon hydrogenated (aSi-H) solar cells grown on a one-dimensional (1-D) dielectric subwavelength gratings improve the short circuit current by a factor of more than 51% when compared with conventional, flat ultrathin aSi-H devices. This improvement is possible due to several mechanisms. In addition the increase in exposed area caused by the nanostructured surface, a reliable computational electromagnetic evaluation of the interaction of the solar spectrum with the cell structure demonstrates that absorption at the active layer is enhanced and also reflectivity is decreased. In addition, the absorbed power at the nonactive layers is larger, helping to increase the temperature and mitigate the Staebler–Wronski effect. The detailed analysis of the power flux inside the structure has also shown that funneling and guiding mechanism are at play, increasing the optical path within the active layer that produces a better performance of the cell.
[DOI: 10.1117/1.JPE.7.017002]

Keywords: ultrathin aSi-H solar cell; nanostructures; light funneling.

Paper 16125 received Nov. 24, 2016; accepted for publication Feb. 10, 2017; published online Mar. 9, 2017.

1 Introduction

Amorphous silicon hydrogenated (aSi-H) solar cells are extensively studied using both modeling and experimental approaches, reporting conversion efficiency larger than 10%.[1] Although these values are well below the record efficiencies in solar photovoltaic conversion, this type of solar cells represents a low-cost solution. The thickness of the active layer in commercial aSi-H solar cells is established around 350 nm. However, ultrathin aSi-H solar cells (with i-aSi-H active layer thickness 150 nm or lower) present advantages in terms of its cost-effectiveness compared with bulk crystalline-based technologies. In addition, this technology could be applied to flexible and lightweight designs, using smaller quantities of materials.[2] The enhancement of its performance is still driving research efforts to make aSi-H solar cells competitive against other solar cell technologies. Actually, two major challenges need to be properly addressed to obtain better performance aSi-H thin and ultrathin film solar cells: a quantitative increase in absorption leading to large photogeneration of charge carriers and a reduction of the Staebler–Wronski effects (SWE) appearing in this material.[3]

Several light trapping geometries and plasmonic effects are proposed to enhance the absorption in solar cells.[4–8] The analysis of the performance has to take into account not only the active layer where photogeneration is produced but also the auxiliary layers including electric contacts. These layers are of importance when considering the overall performance of the cell and cannot be neglected or forgotten in the modeling and simulation. Actually, an easy way to improve performance and increase absorption at the active layer is to decrease the thickness of the front ITO contact combined with the use of plasmonic nanoparticles or structures. This reduction

*Address all correspondence to: Javier Alda, E-mail: javier.alda@ucm.es

1947-7988/2017/$25.00 © 2017 SPIE

in thickness is justified to take advantage of the near-field enhancement associated with plasmonic structures and also to reduce the absorption within this layer. However, thickness values below 30 nm may compromise the front-contact conductivity.[9] Also, n- and p-Si buffer layers are relevant when calculating the optical absorption at the active intrinsic layer and the total absorption of the whole multilayer structure. Finally, the proposal has to be simple and able to be fabricated to allow its development and practical use. Therefore, sophisticated structures could lead to larger efficiency but remain beyond practical realization.[10–14]

In this contribution, we cover all these previous issues. First, we have included every layer in the cell, considering those dimensions previously reported for optimized flat and textured cells.[6] Our simulations have been done using COMSOL multiphysics and incorporating the available material optical properties. The proposed geometry is extruded from a one-dimensional (1-D) profile that uses silicon nitride (Si_3N_4) to pattern the proposed structure. This geometry is applied to the substrate, and the multilayer solar cell arrangement is conformally grown on it. From a simple geometrical point of view, the proposed geometry increases the exposed area of the cell, and at the same time, maintains a small thickness that helps to collect photogenerated carriers before they are trapped or recombined in defect sites, or scattered away from the active layer. The results obtained from our simulations are tested positively and compared with previous experimental findings and modeled designs. At the same time, we considered that the fabrication of the proposed structure can be realized using various techniques such as nanoimprint and etching process, and optical- or electron-beam based lithographic techniques, which are suitable for large area fabrication and produce structures having an aspect ratio similar to those proposed in this contribution.[15–19]

Section 2 establishes the reference results obtained from the computational electromagnetic model of the ultrathin aSi-H structure and serves as a benchmark to validate the model. The proposed 1-D nanostructure is presented in Sec. 3. Section 4 describes how this structure is optimized, maximizing the short circuit current, by changing the geometric parameters of the 1-D profile and by choosing the appropriate material for the patterned scaffold. The optimization of the structure by maximizing short circuit current is reported by most of studies that deals with similar approaches.[20–22] This is done because the short circuit current is a parameter that is easily related to enhancement in the absorption efficiency caused by light trapping mechanisms. The explanation of the enhanced performance in terms of funneling and guiding mechanisms is given in Sec. 5. Finally, Sec. 6 summarizes the main conclusions of this contribution.

2 Computational Electromagnetism Applied to aSi-H Solar Cells

An aSi-H thin film solar cell has a multilayer structure that is organized from bottom to top as follows [see Fig. 1(a)]: Ag/AZO/n-aSi-H/i-aSi-H/p-aSi-H/ITO, where the back contact layer is made of Ag. AZO denotes the aluminum zinc oxide buffer layer that prevents the diffusion of the back contact metal into the semiconductor layer. The junction layers pin-aSi-H are arranged to have the p- and n-layers establishing an internal electric field that collects the photogenerated carriers at the i-aSi-H active layer. These layers also reduce resistivity losses by forming ohmic contacts between the intrinsic layer and the collecting contacts. Finally, ITO corresponds with the indium tin oxide that is the transparent front contact layer. The optical constants used in our calculations have been extracted from Vora et al.[6]

The spectral absorption rate can be calculated as

$$A(\omega) = \frac{1}{2}\omega\varepsilon''|E(\omega)|^2, \tag{1}$$

where ω is the angular frequency of the incoming radiation, ε'' is the imaginary part of the dielectric permittivity of the material, and $E(\omega)$ is the electric field. The absorption rate is defined as the ratio of the absorbed power to the incident power and can be used to calculate the absorptance at each individual layer of the cell. Actually, this absorption is made by integrating over the interaction volume of each layer. As far as we are interested in optical absorption at the i-aSi-H layer for an incoming broadband radiation, we need to evaluate this absorbed power density as

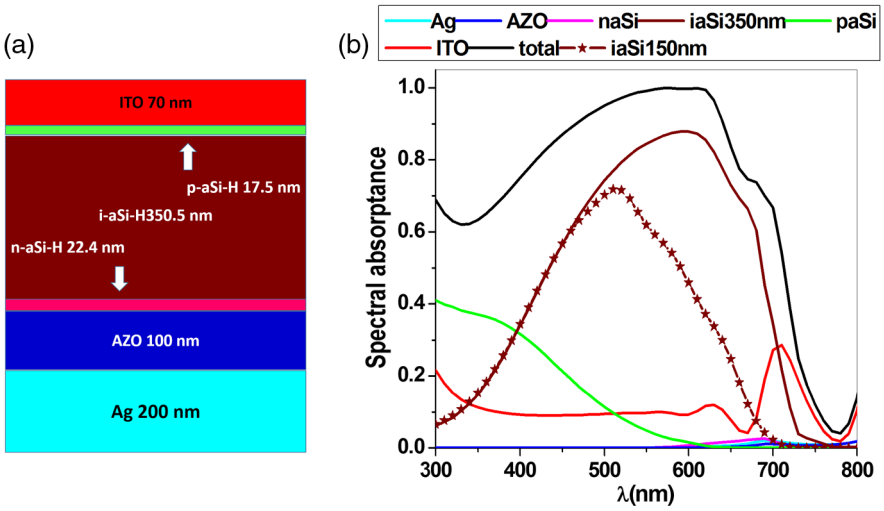

Fig. 1 (a) Diagram of the flat reference cell. (b) Spectral absorptance of each individual layer in the cell.

$$P^{i}_{\text{abs}} = \int A(\omega)\Phi_{AM1.5}(\omega)\mathrm{d}\omega, \tag{2}$$

where $\Phi_{AM1.5}(\omega)$ is the spectral irradiance as a function of frequency.[23] Although Eqs. (1) and (2) are given in terms of the angular frequency, it is also customary in optics to express spectral characteristics in terms of the wavelength, λ. In a solar cell, we are also interested in knowing the short circuit current, J_{SC}, circulating through the structure as a function of the solar irradiance. This parameter is the one that we need to improve when optimizing a solar cell structure. Assuming that each absorbed photon will create one electron-hole pair contributing to the short circuit current, J_{SC} can be given in terms of the wavelength as

$$J_{SC} = \int \frac{q}{hc} A(\lambda)\lambda\Phi_{AM1.5}(\lambda)\mathrm{d}\lambda, \tag{3}$$

where q is the electron charge, c is the speed of light in vacuum, and h is the Planck's constant. The absorption term, $A(\lambda)$, in Eq. (3) refers to the absorption at the i-aSi-H active layer, where the photocurrent is generated. The absorbed power at the other layers of the cell is mainly converted as heat due to dissipative losses and recombination due to the short diffusion length and low mobility of minority carrier, and to the high density of defect states.[6,24–27]

Our simulation model has been tested by calculating the spectral absorption at each individual layer for the following structure: Ag 200 nm/AZO 100 nm/n-aSi-H 22.5 nm/i-aSi-H 350 nm/p-aSi-H 17.5 nm/ITO 70 nm, where the numbers represent the thickness of each layer. The results are presented in Fig. 1(b), and the obtained short circuit current is $J_{SC} = 11.7\ \text{mA/cm}^2$, which is the same result given by Vora et al.[6] The absorbed power at each layer depends on its optical properties and thickness, and it is limited by its band gap, so different material with different optical properties and arranged with different thicknesses absorb light differently.[28–31] In addition, the absolute amount of absorbed light at a given layer depends on the amount of light that is actually reaching it. These reasons explain the different contributions to the absorbed power along the cell structure. Then, after validating our model against previous results,[6] we have considered an ultrathin aSi-H solar cell structure with the following parameters: Ag 200 nm/AZO 15 nm/n-aSi-H 22.5 nm/i-aSi-H 150 nm/p-aSi-H 17.5 nm/ITO 70 nm, where the thickness of the active layer is reduced to only 150 nm. This thinner active layer will reduce the effect of defect states on the cell performance.[32] In this ultra-thin structure we also reduce the thickness of the AZO layer to facilitate the conformal deposition of other layers. The spectral absorption in the i-aSi-H layer for this structure is shown in Fig. 1(b), which accounts for only $J_{SC} = 8.98\ \text{mA/cm}^2$. This low value is due to the reduction of the thickness of

the active layer. In addition, optical power reaches the back layers that also contribute to the reduction in absorption.

3 One-Dimensional Nanostructure Profile for aSi-H Cells

Texturing the geometry of the front or back contacts at the nanoscale has been proposed to enhance the trapping of light inside the active layer of the cell. This approach requires the combination of an optimum geometry and an appropriate material choice compatible with the cell structure, maintaining a good optical and electric behavior. One of the simplest solutions is to extrude, or elongate, an 1-D profile with the easiest possible geometry and parameterization. Our first choice of material to work as a scaffolding of this structure has been Si_3N_4. This dielectric material is used to create a textured surface over the back contact of the structure. Once this nanostructure is built, it can act as a pattern to grow the multilayer cell arrangement conformally. One of the reasons why this approach is advantageous for solar cells is the increase in exposed surface when considering this geometry. In addition to that, light traveling along the active ultrathin layer propagates longer and will be better absorbed than for flat, unstructured ultrathin cell. To illustrate this fact, we may analyze the increase in exposed area when having a triangular shape with the following geometrical parameters: H is the height of the triangular shape, B_w is the transverse width of the triangle (length of the base), and p is the repetition period. For a structured surface, we replace the flat interface by a triangular profile. The new width of the exposed profile will be B_w plus the sum of layers on both sides of the grating (AZO- n-aSi-H and i-aSi-H), over a period p. This value is equal to 375 nm. These geometrical parameters are shown in Fig. 2(a). The new length of the profile will be

$$L = (p - B_w - 375) + 2\sqrt{\left(\frac{B_w + 375}{2}\right)^2 + H^2}\ \text{nm}, \tag{4}$$

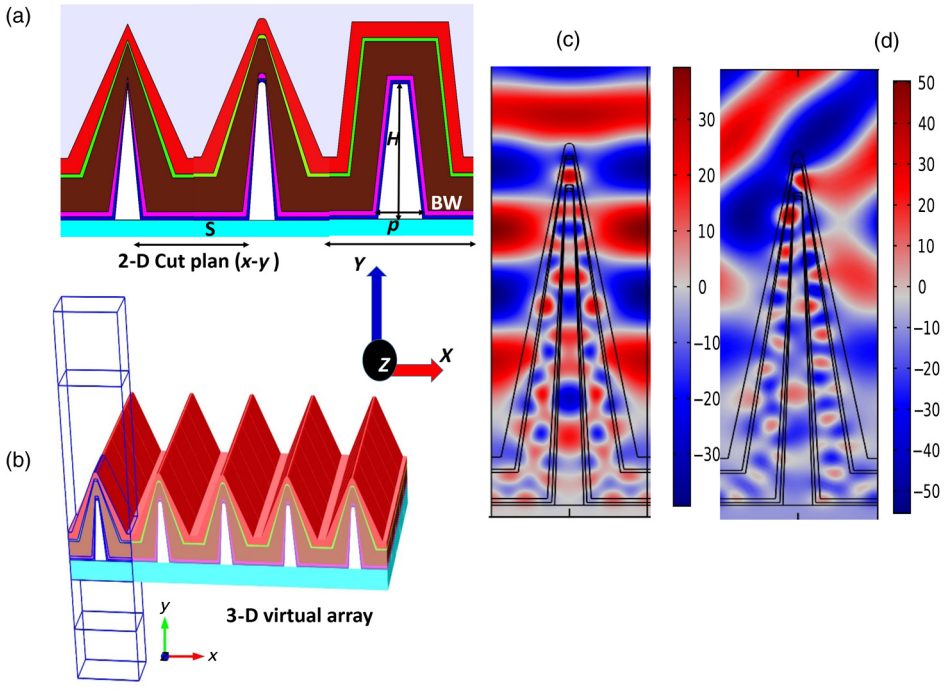

Fig. 2 (a) 2-D unit cell cross section over the $X - Y$ plane. (b) 3-D representation of the proposed structure showing the unit cell used in the numerical calculation. (c) Map of the transverse electric field for normal incidence conditions at $\lambda = 630$ nm. (d) Map for the electric field distribution for a plane wave incident at a angle of 50 deg for $\lambda = 630$ nm.

which should be compared with p to obtain the increasing in the exposed area that is proportional to L/p. Just by considering this parameter, the optimization of the nanostructure produces high aspect ratio geometries that may become difficult to fabricate. Therefore, this approach has to be combined with a detailed calculation of the interaction between light and active realizable structures.

Figure 2(a) shows three profiles of the textured structure in the XY plane. The one on the left is a pointed triangular shape that has its culprit rounded in the second geometry. This geometry is closer to the one that could actually be fabricated. However, the replacement of the pointed triangle by a rounded tip is not very significant in the overall performance of the structures. The third geometry has a trapezoidal shape. In Fig. 2(b), we have represented a 3-D view of the triangular proposed geometry where the calculation domain is also superimposed. Within this calculation cell, it is possible to evaluate the electromagnetic quantities of interest. Figures 2(c) and 2(d) show the transverse component of the electric field for two cases of interest at $\lambda = 630$ nm, having two angles of incidence $\theta = 0$ deg and $\theta = 50$ deg. Actually, when evaluating the radiation at the bottom of the structure, we may see that energy is trapped within it, reinforcing the optical power at the intrinsic layer. Figure 2(d) shows the electric field distribution for oblique incidence, $\theta = 50$ deg at $\lambda = 630$ nm. In this case, we can check how the wave propagates through the structure, especially at the intrinsic aSi-H layer.

When considering the spectral absorption of the structure, the unit cell will be illuminated with an irradiance distribution that follows a model of the solar spectrum given by the spectral irradiance function, $\Phi_{AM1.5}(\lambda)$.[23] From Fig. 1(b), we can see that absorption is happening at every layer of the cell, especially at the front layers where the irradiance is higher. The absorption enhancement in the i-aSi-H layer will mainly contribute to the photogenerated current. However, the parasitic absorption enhancement in other layers will be dissipated as heat, which will reinforce a self-annealing mechanism of the device leading to a reduction of the SWE.

4 Optimization

Until here, we have discussed the advantage of the 1-D elongated dielectric structure in light trapping and SWE defects repair, now we discuss the optimization of the structure when changing the geometric parameters and the material choice. Although we select the triangular shape for the optimization process, we checked the validity of this optimization for other shapes (rectangular and trapezoidal). To ease the first optimization step, we fix the grating height at $H = 300$ nm as a starting value, then make the optimization process for the grating base width (B_w) and grating separation, S. These geometrical parameters are related as $p = S + B_w$, where p is the profile period. In Fig. 3(a), we have calculated optimum values for the geometrical profile $B_w = 150$ nm and $S = 650$ nm. At the same time, there exists other combinations of S and B_w providing values close to the maximum one, as it has been denoted with circles at Fig. 3(a). Then, it should be possible to choose geometric parameters complying better with fabrication constrains. This optimization shows that not only an increase in the exposed surface area is important. Only after evaluating the interaction of the incoming light with the materials and geometries expressed here is it possible to optimize the short circuit current circulating across the cell. Figure 3(b) shows the enhancement in the surface area exposed to light, with changing the same geometrical parameters, while fixing the height at 1800 nm. Although the optimum geometric values for the short circuit current and for the maximum surface area are close, they are not coincident, meaning that the surface area is not the only parameter that controls the performance of the structure. Therefore, the material choice, the geometry of the structure, and the layer arrangement are determinant parameters when enhancing the performance of the device.

In the previous calculation, the height, H, was fixed at 300 nm to optimize other parameters (B_w and S). Now, the optimization of the height is made by considering the optimized values of B_w and S previously obtained for the triangular and trapezoidal cases. Using the previously presented model, we can evaluate numerically the dependence of J_{SC} with respect to H. The results are shown in Fig. 3(c), where J_{SC} increases rapidly with H, until reaching a saturation level. This happens because most of the optical power is absorbed at the top portion of the

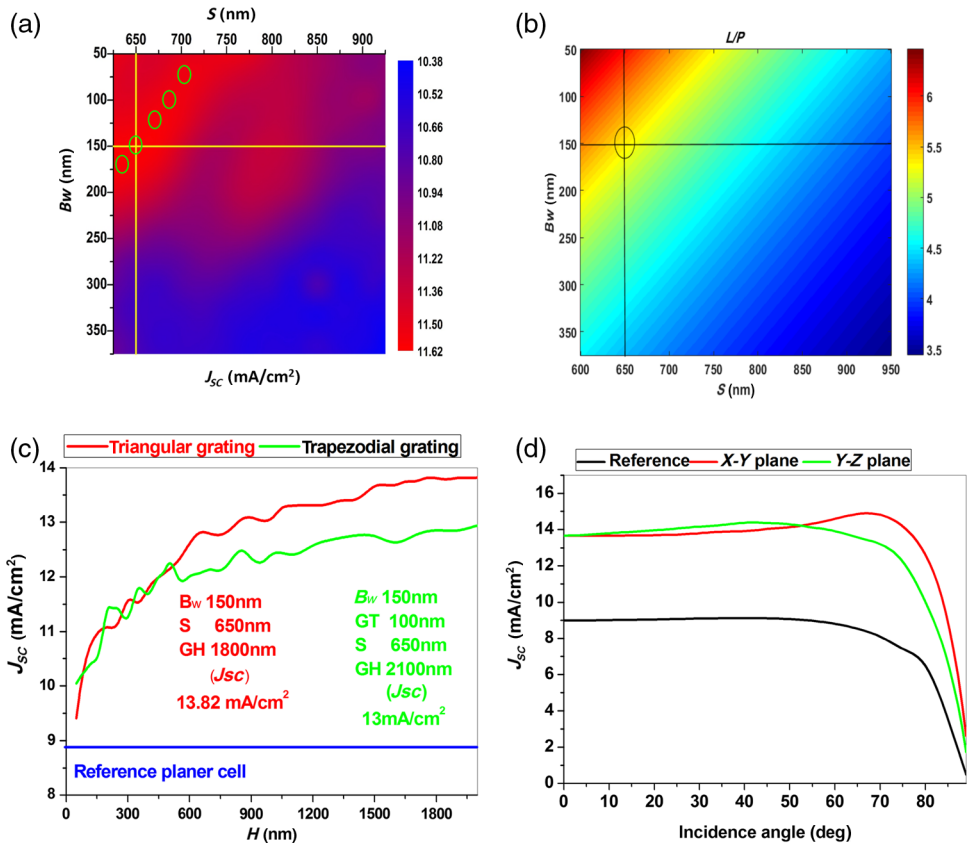

Fig. 3 (a) Short circuit current, J_{SC}, as a function of B_w and S. (b) Enhancement in the exposed area of the cell in terms of B_w and S. (c) Short circuit current as a function of H for the optimum case evaluated from map (a) and for two possible geometries. (d) Short circuit current as a function of the angle of incidence for the optimum design.

nanostructure, and by increasing the height of the triangle, there is no substantial improvement of J_{SC} when reaching the bottom of the structure. Actually, the saturation level occurs for values around 1800 nm for both geometries. When compared with the flat reference aSi-H, we can see that the nanostructure cell increases absorption by a factor of more than 51% for large H values, having a very similar dependence and values for the triangular and trapezoidal cases until reaching $H = 600$ nm. Table 1 summarizes the short circuit current for the flat reference cell and optimized pattern cell for TE and TM polarization and average cases.

When dealing with low-cost solar cells, we should also pay attention to the dependence of its performance with respect to the angle of incidence. This is even more important when no active tracking is deployed. Typically, J_{SC} decreases strongly when the angle of incidence is large. In addition, for the elongated structure proposed here, the dependence varies with the polarization state and the orientation of the plane of incidence with respect to the profile. Taking all these

Table 1 Short circuit current for reference flat cell and optimized textured cell. Transversal electric (TE) and transversal magnetic (TM) represent the two possible polarization orientations.

J_{SC} (mA/cm^2)	Percentage	Structure
8.98	—	Reference flat
13.45	49.78%	Textured TM
13.82	53.90%	Textured TE
13.64	51.89%	Textured average

previous conditions and situations into consideration in Fig. 3(d), we have plotted the values of J_{SC} for the case of a nanostructured cell for two possible orientations of the plane of incidence. In this same plot, we have also included the angle dependence obtained for a reference flat solar cell.[6] From these results, besides the wide angle of acceptance, we can see an increase in the short circuit current that reaches a maximum value of $J_{SC} = 14.4$ mA/cm^2 and $J_{SC} = 14.8$ mA/cm^2 for incidence within the YZ plane and for the XY plane of incidence cases, respectively. These results average the TE and TM polarization.

4.1 *Effect of Different Materials When Applied to the Structure*

Not only are the design and shape important parameters to optimize the performance of solar cells but also an appropriate choice of materials makes possible an improvement in the capabilities of the device. To show this, we have evaluated the performance of the structure when different materials are used for the fabrication of the grating pattern where the cell structure is deposited on. We have seen that a material with high n value and low k value performs better in this structure (being n and k the real and imaginary parts of the index of refraction). A small k is responsible for less absorption at the scaffolding structure. A large value of n contributes to a better funneling because light propagation tends to be perpendicular to the interface, promoting better propagation within the active layer. To prove that, we have evaluated the short circuit current of the device using different materials for the grating: Ag, AZO, SiO_2, and Si_3N_4. As we pointed out previously, materials with high n values alter the electric field distribution at the interface and help to trap light inside the structure. At the same time, when computing the power available at each layer, materials with high k values will absorb more light and decrease the total amount of optical power available for absorption at the i-aSi-H layer.

We calculated the absorption inside the grating for the proposed materials. Figure 4(a) shows the spectral absorption inside the grating only, and the relative share of this absorption of the grating scaffold itself in the absorption process. The cell with optimized grating from Ag gives a short circuit current of $J_{SC} = 12.66$ mA/cm^2; for AZO, we find a value of $J_{SC} = 13.3$ mA/cm^2; for SiO_2, the short circuit current is $J_{SC} = 13.4$ mA/cm^2; and for Si_3N_4, we obtain $J_{SC} = 13.64$ mA/cm^2. These previous results already average the TE and TM polarization. The values of short circuit current for the cell using a grating of Si_3N_4, AZO, and SiO_2 are close to each other because the refractive index of them are similar, but AZO has little absorption and SiO_2 has lower refractive index. Then, following the previous reasoning and result, we find that Si_3N_4 is the better choice to manufacture the proposed profile. In Fig. 4(a), the metallic grating accounts for significant absorption in the effective absorption band of the cell (300 to 720 nm) showed by the vertical line, this absorption will decrease the total absorption efficiency of the cell, especially for the ultrathin layer arrangement optimized here. A broadband absorption behavior is shown in Fig. 4(b), where the absorption at the i-aSi-H layer is higher than that of the reference flat cell at all wavelengths inside the absorbing band of the material, which extends from 200 to 800 nm.

As mentioned previously, the enhancement is not only in the i-aSi-H active layer but also in all other layers. In Fig. 4(c), We show the absorbed power budget in each individual layer for different structures, and the portion of absorption that will be mostly generate a photocurrent. The total absorbed power in all layers and the absorbed power inside the i-aSi-H layer only are summerized in Table 2. The significant absorption enhancement caused in nanostructured cell is shared by the ITO, p-, and n-aSi-H layers, producing heat by dissipation and recombination as shown in Fig. 4(b). This heat will partially mitigate the SWE.[6,33]

The performance of the structure using different material for the grating profile can be explained by sweeping for the short circuit current in terms of the refractive index of the grating. This analysis can be done by considering a dielectric material with very low absorption, or no absorption, in the band of interest of the active layer material. This assumption is valid for many dielectric materials, and therefore, we can cancel the imaginary part of the refractive index and vary only for the real part. The results are shown in Fig. 4(d), which will agree with our previous explanation. This plot shows that a value of 2.2 defines a change between high and low enhancements. This is one of the reasons for selecting Si_3N_4 as appropriate material for these structures.

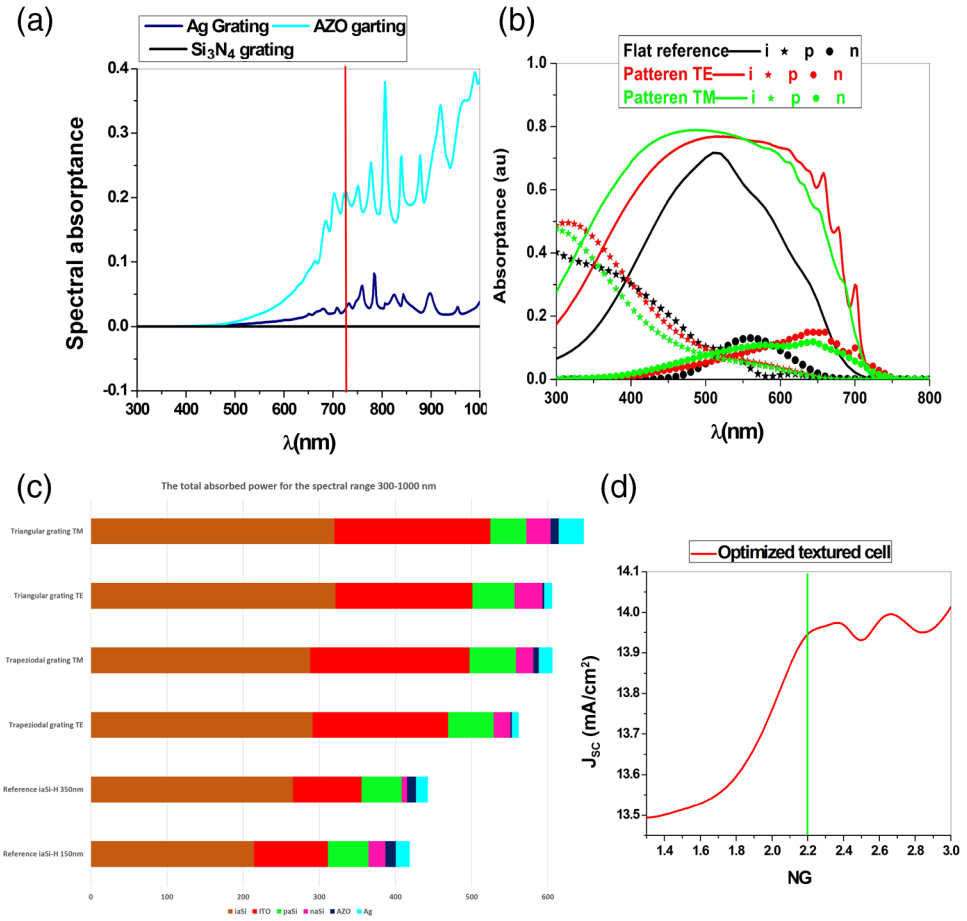

Fig. 4 (a) Absorption inside grating only for different materials. (b) Spectral absorptance in i-aSi-H layer for the reference flat cell and textured cell TE and TM polarizations. (c) Absorbed power in each individual layer for different structure. (d) Short circuit current of the optimized solar cell with grating of different refractive indices.

Table 2 Absorbed power distribution.

	Absorbed power W/m^2	
Structure	Total	in i-aSi-H only
Reference flat i-aSi-H 150	418.77	214.21
Reference flat i-aSi-H 350	442.34	265.24
Trapezoidal pattern cell	583.90	290
Triangular pattern cell	626.56	320

5 Funneling and Guiding Effects

Light funneling is one of the light trapping mechanisms, which is expected to be intensively applied to solar cell for performance improvements. Previous contributions show that this mechanism is at work in multilayer metal-dielectric structures.[34,35] However, metallic layers combined with dielectric layers that can produce light funneling effects will account for both high reflections from the metal surface and high absorption inside the metal itself. In our case, we could produce a similar effect with high aspect ratio dielectric structures. Figure 5 shows the case of the optimized structure for three wavelengths and two orthogonal

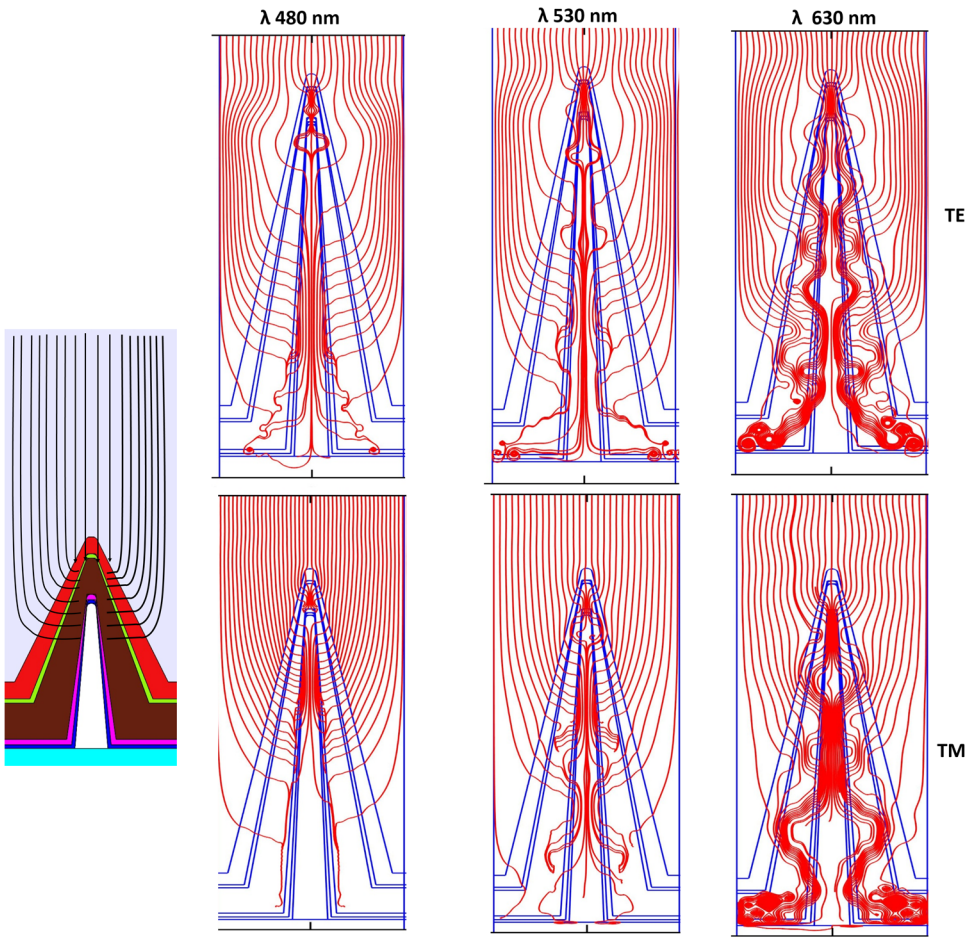

Fig. 5 The left graph shows a schematic picture of the structure that represents how incoming light is diverted toward the inner layers. The rest of the plots show the Poynting vector flux for three wavelengths $\lambda = 480$, 530, and 630 nm and two orientations of the electric field. Funneling appears in every plot and guiding in the active layer is stronger at $\lambda = 630$ nm.

orientations of the electric field. These plots represent the Poynting vector flux. From these plots, we can check how the incoming flux move toward the structure and, at some specific wavelengths, light is guided within the active layer (see for example, the case of $\lambda = 630$ nm in Fig. 5).

6 Conclusions

Low-cost solar cells, as those made with amorphous Si, can compete better with other technologies and improve its performance when including nanostructures properly adapted to the design and function of these elements. We have seen that an extruded profile that serves as a geometrical pattern to grow the solar cell layer improves notably the short circuit current delivered by the cell. The optimization of the proposed geometry has taken into account not only the typical layer deposition of aSi-H cells but also those constrains derived from a conformal deposition of the constituent layers of the cell. Then, the proposed improvement can be fabricated in two steps. In the first step, the grating scaffolding is built on a flat surface using the available techniques: e-beam lithography and etching, or nano-imprinting. After the relief is made, the thin or ultrathin aSi-H cell structure is successively deposited on it. This approach makes easier the nanostructuring of the surface of aSi-H cells because once the grating profile is made, the same standard deposition strategy used for flat surface solar cells can be applied to produce the final device. Then, nanostructuring is provided from the very beginning, avoiding a

more delicate nanostructure patterning if applied to the last deposition of the already fabricated cell.

Using computational electromagnetism tools, it is possible to evaluate the short circuit current delivered by a variety of designs and conditions. This capability has been used to optimize the geometrical parameters of the proposed designs, analyzing at the same time the intrinsic dependence with wavelength, polarization, relative orientation of the incidence plane, and angle of incidence. In all the proposed geometry and materials analysis, we have seen how the nanostructure is able to enhance the short circuit current well above the reference level of the flat solar cell. In addition, improving absorption at the intrinsic active i-aSi-H layer, the proposed geometry also increases absorption at other auxiliary layers that partially converts radiation into heat. This conversion can mitigate partially the defects caused by the SWE.

Summarizing the results of this contribution, we can say that nanostructuring the geometry of the cell produces an improvement of the performance of the cell that could make this low-cost technology better positioned in some areas and environments.

Acknowledgments

This work was partially supported by the Egyptian Ministry of Higher Education missions section under Egyptian cosupervision grant at University Complutense of Madrid, Spain. We would like to thank the Egyptian Institute, Cultural Office of the Egyptian Embassy in Madrid, Spain. This work has been partially supported by project TEC2013-40442 from the Spanish Ministerio de Economia y Competitividad.

References

1. M. A. Green et al., "Solar cell efficiency tables (version 45)," *Prog. Photovoltaics Res. Appl.* **23**(1), 1–9 (2015).
2. V. E. Ferry et al., "Optimized spatial correlations for broadband light trapping nanopatterns in high efficiency ultrathin film a-Si: H solar cells," *Nano Lett.* **11**(10), 4239–4245 (2011).
3. D. Staebler and C. Wronski, "Reversible conductivity changes in discharge-produced amorphous Si," *Appl. Phys. Lett.* **31**(4), 292–294 (1977).
4. J. N. Munday and H. A. Atwater, "Large integrated absorption enhancement in plasmonic solar cells by combining metallic gratings and antireflection coatings," *Nano Lett.* **11**(6), 2195–2201 (2011).
5. Y. Li et al., "3D simulation of morphological effect on reflectance of Si3N4 sub-wavelength structures for silicon solar cells," *Nanoscale Res. Lett.* **7**(1), 1–6 (2012).
6. A. Vora et al., "Multi-resonant silver nano-disk patterned thin film hydrogenated amorphous silicon solar cells for Staebler–Wronski effect compensation," *J. Appl. Phys.* **116**(9), 093103 (2014).
7. H. Xiao et al., "Performance optimization of flexible a-Si: H solar cells with nanotextured plasmonic substrate by tuning the thickness of oxide spacer layer," *Nano Energy* **11**, 78–87 (2015).
8. Y. Y. Cheng et al., "Increased upconversion performance for thin film solar cells: a trimolecular composition," *Chem. Sci.* **7**(1), 559–568 (2016).
9. J. Gwamuri et al., "A new method of preparing highly conductive ultra-thin indium tin oxide for plasmonic-enhanced thin film solar photovoltaic devices," *Sol. Energy Mater. Sol. Cells* **149**, 250–257 (2016).
10. S. Pillai et al., "Surface plasmon enhanced silicon solar cells," *J. Appl. Phys.* **101**(9), 093105 (2007).
11. Y. Cui et al., "A thin film broadband absorber based on multi-sized nanoantennas," *Appl. Phys. Lett.* **99**(25), 253101 (2011).
12. I. Massiot et al., "Nanopatterned front contact for broadband absorption in ultra-thin amorphous silicon solar cells," *Appl. Phys. Lett.* **101**(16), 163901 (2012).

13. M. F. Nezhad, N. Shahtahmassebi, and M. Behdani, "Improvement efficiency of thin-film solar cell by plasmonic properties of silver," *Opt. Int. J. Light Electron. Opt.* **127**(20), 8419–8422 (2016).
14. S. Saravanan and R. Dubey, "Optical absorption enhancement in 40 nm ultrathin film silicon solar cells assisted by photonic and plasmonic modes," *Opt. Commun.* **377**, 65–69 (2016).
15. J. J. Wang et al., "Ultraviolet wave plates based on monolithic integration of two fully filled and planarized nanograting layers," *Opt. Lett.* **31**(12), 1893–1895 (2006).
16. K. J. Morton et al., "Wafer-scale patterning of sub-40 nm diameter and high aspect ratio (>50:1) silicon pillar arrays by nanoimprint and etching," *Nanotechnology* **19**(34), 345301 (2008).
17. Y. Sharma and A. Dhawan, "Plasmonic nano-fingers on nanowires as SERS substrates," *Opt. Lett.* **41**(9), 2085–2088 (2016).
18. Y. Zheng et al., "Alignment method combining interference lithography with anisotropic wet etch technique for fabrication of high aspect ratio silicon gratings," *Opt. Express* **22**(19), 23592–23604 (2014).
19. Y. J. Shin, Y.-K. Wu, and L. J. Guo, "Nanoimprinting ultrasmall and high-aspect-ratio structures by using rubber-toughened UV cured epoxy resist," *Nanotechnology* **24**(25), 255302 (2013).
20. D. Kataria and S. S. K. Iyer, "Optimization of MoO_3 buffer layer thickness for short circuit current enhancement in Ag nanoparticle incorporated CuPc solar cell," in *Proc. IEEE 42nd Photovoltaic Specialist Conf. (PVSC)*, pp. 1–6 (2015).
21. J. Lee et al., "Enhancement of the short circuit current in organic photovoltaic devices with microcavity structures," *Appl. Phys. Lett.* **97**(8), 187 (2010).
22. M. Ghebrebrhan et al., "Global optimization of silicon photovoltaic cell front coatings," *Opt. Express* **17**(9), 7505–7518 (2009).
23. NERL, "Spectral solar irriadiance," http://rredc.nrel.gov/solar/spectra/am1.5/ (30 November 2016).
24. Z. C. Holman et al., "Current losses at the front of silicon heterojunction solar cells," *IEEE J. Photovoltaics* **2**(1), 7–15 (2012).
25. J. Poortmans and V. Arkhipov, Eds., *Thin Film Solar Cells: Fabrication, Characterization and Applications*, pp. 208–209, John Wiley & Sons, West Sussex, England (2006).
26. N. Sahraei et al., "Investigation of the optical absorption of a-Si: H solar cells on micro-and nano-textured surfaces," *Energy Procedia* **33**, 166–172 (2013).
27. R. Varache et al., "Front side recombination losses analysis in rear emitter silicon heterojunction solar cells," *Energy Procedia* **55**, 302–309 (2014).
28. A. Belfar, "The role of p^+-layer dopant concentration, p^+-layer band gap and p^+-layer thickness in the performances of a-Si: H $n-i-p-p^+$ solar cells with double layer window nanocrystalline silicon," *Opt. Int. J. Light Electron Opt.* **126**(24), 5688–5693 (2015).
29. J. Müllerová et al., "A study of optical absorption in amorphous hydrogenated silicon thin films of varied thickness," *Appl. Surf. Sci.* **256**(18), 5667–5671 (2010).
30. S. Hasegawa and Y. Imai, "Thickness dependence of electrical and optical properties and ESR in undoped a-Si: H," *Philos. Mag. B* **46**(3), 239–251 (1982).
31. J.-W. Shin et al., "The properties of a-Si: H pin solar cell by intrinsic layer's thickness," *Mol. Cryst. Liq. Cryst.* **551**(1), 257–263 (2011).
32. P. Chaudhuri et al., "Thickness dependence of light-induced effects in a-Si solar cells," *Sol. Cells* **31**(1), 13–21 (1991).
33. M. Pathak, J. M. Pearce, and S. Harrison, "Effects on amorphous silicon photovoltaic performance from high-temperature annealing pulses in photovoltaic thermal hybrid devices," *Sol. Energy Mater. Sol. Cells* **100**, 199–203 (2012).
34. P. Zhu et al., "Funneling light into subwavelength grooves in metal/dielectric multilayer films," *Opt. Express* **21**(3), 3595–3602 (2013).
35. M. Mivelle et al., "Light funneling from a photonic crystal laser cavity to a nano-antenna: overcoming the diffraction limit in optical energy transfer down to the nanoscale," *Opt. Express* **22**(12), 15075–15087 (2014).

Mahmoud H. Elshorbagy obtained his bachelor's degree in physics in 2007 from Minia University, Egypt, and his MS in the same university working in hybrid solar cells fabrication and characterization. Now he is a PhD student at the Complutense University of Madrid, Spain.

Javier Alda obtained his Licentiate in sciences from the University of Zaragoza, Spain, in 1985 and his PhD at Complutense University of Madrid, Spain, in 1988. He is currently a professor of applied optics at Complutense University. His current main interest is the use of optical antennas and resonant structures in nanophotonics applications. He is a fellow member of SPIE.